Sputtering limits versus signal-to-noise limits in the observation of Sn balls in a Ga^+ microscope

V. Castaldo,[a] C. W. Hagen, B. Rieger, and P. Kruit
Delft University of Technology, Lorentzweg 1, 2628 CJ Delft, The Netherlands

(Received 23 June 2008; accepted 7 October 2008; published 1 December 2008)

In principle, a scanning ion microscope can produce smaller probe sizes than a scanning electron microscope because the diffraction contribution is smaller. However, the imaging resolution is often severely limited by the sputtering damage. In this article, an experimental procedure to establish the limit of a focused ion beam system for imaging purposes is proposed. The procedure is based on the observation of the change in geometry (i.e., shrinking) of the features in a Sn-ball sample imaged with a Ga^+ beam. Plots of the balls' diameter versus the irradiation time give a straightforward visual evaluation of the time allowed for the observation of a single feature before the removal of material due to the ion bombardment becomes unacceptable. For each particle, the curve, together with the error band connected with the imaging process, gives the values of uncertainty/resolution due to the two competing processes, collecting of information (for example, from secondary electrons) and damaging of the target. A plot of the uncertainty that is derived from these two processes for different sampling times allows the determination of the limiting factor of the imaging mode in use, and, ultimately, the highest possible resolution obtainable with a given machine for the observation of a certain sample. Together with simulations and theoretical studies, the described procedure will be able to confirm the effectiveness of the new ion sources that are currently being developed.
 [DOI: 10.1116/1.3013306]

I. INTRODUCTION

Since the development of liquid metal ion sources (LMISs) and their application to focused ion beam (FIB) systems by Seliger *et al.* in 1978,[1] FIBs became more and more widely used, not anymore as mere laboratory instruments, but, thanks to the high brightness, high current, and good reliability of the LMIS, as indispensable tools for the semiconductor industry, in fields of application such as integrated circuit review and modification (assisted etch/deposition, cross-section cut, and implantation), transmission electron microscopy/scanning transmission electron microscopy sample preparation, thin film head manufacturing, and even mass spectrometry.[2,3]

Currently scanning electron microscopes (SEMs) give better results than scanning ion microscopes (SIMs) in terms of resolution and ease of operation. Nevertheless, the use of ions instead of electrons in scanning microscopy promises several advantages: new contrast mechanisms, larger depth of focus, and perhaps higher resolution. Assuming a zero-sized probe, Ohya and Ishitani[4,5] showed that, except for targets of low Z, the lateral distribution of ion-induced secondary electrons (SEs) is much narrower, leading to a better spatial resolution for SIM than for SEM; the same authors concluded that the topographic contrast for heavy materials is clearer in a SIM image than in a SEM image, while for light materials the difference is negligible.[6] Furthermore, Ishitani *et al.*[7] predicted that SIM images are more sensitive to the target-surface state than SEM images.

[a]Electronic mail: v.castaldo@tudelft.nl

A. Theory of sputtering

The main problem, when it comes to imaging with an ion beam, is the sputtering of target atoms: Ions are thousand times more massive than electrons, so the damage to the imaged sample can actually be the limiting factor for the resolution. This issue has been addressed by Orloff *et al.*[8,9]

Defining the resolution is not an easy task. The most popular definition is still the one proposed, for diffraction-limited systems, by Rayleigh in 1879,[10] based on the ability to distinguish two objects in an image [thus, implicitly requiring a sufficient amount of contrast and signal-to-noise ratio (SNR)].

More quantitative definitions involve the notion of the optical transfer function, defined as the Fourier transform of the point spread function (which describes the response of an imaging system to a point source or point object) or, in the case of electron-optical systems, as the Fourier transform of the current density distribution.[2] A relatively simple way to define the resolution in an electron-optical system is assuming that it is equal to the size of the focused beam, which is in turn quite difficult to determine. Following Ref. 2 or Ref. 11, this can be calculated adding the contributions from the source image, the spherical aberration, and the chromatic aberration. More complete expressions for d, taking into account also the contributions of diffraction, Coulomb interaction, Boersch effect, etc., can be found in literature.[12,13]

None of these definitions is fully satisfying for a FIB, in which the beam can destroy an object before an adequate amount of signal is detected. This limit must be taken into account when defining the resolution for such a system. From geometric reasoning, considering that the beam can

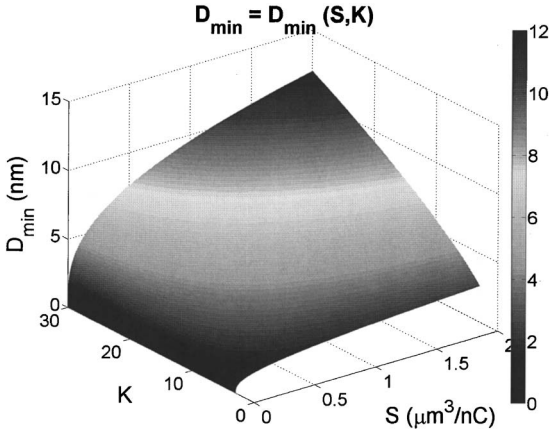

FIG. 1. Minimum detectable feature in a FIB imaging system from Eq. (1), as a function of sputtering sensitivity S and signal-to-noise ratio K, for $\delta=2$ and $\Omega=0.5$.

overlap itself during the scan of an image, and assuming that both the primary ion beam and the SEs are Poisson distributed, that all the SEs are collected, and that there are no other sources of noise in the system, Orloff *et al.*[9] proposed the following definition of resolution in a FIB:

$$D_{\min}=\sqrt[3]{\frac{eSK^2(1+\delta)}{\Omega^2\delta}}, \tag{1}$$

where D is the feature size, K is the signal-to-noise ratio, δ is the SE yield, Ω (scan-step-size/beam-diameter) is a measure of the overlap, and S (in $\mu m^3/nC$) is the "sputtering sensitivity," defined as

$$S=\frac{YA}{\rho N_0 e}, \tag{2}$$

where ρ and A are the target density and atomic weight, N_0 is Avogadro's number (6.02×10^{23} at./mol), and Y is the sputter yield (sputtered atoms/primary ion). A plot of Eq. (1), showing $D_{\min}$ as a function of S and K, is in Fig. 1. It can be useful to express $D_{\min}$ as a function of scanning time instead of SNR. This is straightforward, under the same assumptions for which Eq. (1) holds,

$$K=\sqrt{\frac{N_i\delta}{1+\delta}}=\sqrt{\frac{\delta}{1+\delta}\frac{I_{\text{beam}}}{epx}t_{\text{scan}}} \tag{3}$$

and

$$D_{\min}=\sqrt[3]{\frac{eS}{\Omega^2}\frac{I_{\text{beam}}}{epx}t_{\text{scan}}}, \tag{4}$$

where N_i is the number of primary ions per pixel, I_{beam} is the ion current, and px is the total number of pixels in the image. Equations (3) and (4) are written for single charged ions; should this be not the case, the electron charge e must be multiplied by the order of ionization.

It appears that, while for extended structures there are several limiting mechanisms such as rearrangement and redeposition, for small particles, in the order of a few nanometers, the imaging resolution is actually determined by the competition between sputtering and SE production/collection. This is indeed the case in the present FIB systems, most of which exploit beams of Ga^+ (atomic weight: 69.723), whose high sputtering power represents the fundamental limit to the resolution. The only way to obtain higher performances in terms of resolution and collectable SNR is exploiting sources of low mass ions, such as H^+ and He^+.

B. New ion sources

In the past few years, much effort has been directed to the design of novel ion sources, expecially for imaging purposes (see Ref. 14 for a review). The "perfect ion source" will be able to overcome the drawbacks connected with the use of LMISs (high energy spread, $\Delta E/E\sim2\times10^{-4}$, leading to high chromatic aberration; strong sputtering of the sample; and permanent implantation of metal ions, which can change the electrical and/or magnetic properties of the specimen under inspection) while keeping its advantages (high reduced brightness, in the order of 10^6 A/m^2 sr V; high current stability; and long lifetime). Presently LMISs remain state-of-the-art ion sources, being unsurpassed in terms of robustness and reduced brightness. Recently ALIS Corporation developed a new helium microscope, which is expected to produce as small a spot size as 0.25 nm, thanks to a high predicted source brightness ($B>10^9$ A/cm^2 sr), low energy spread ($\Delta E/E\sim2\times10^{-5}$), and small diffraction effects.[15] Whether or not this new microscope fulfills these expectations, the excitement about novel ion sources makes a procedure capable of characterizing ion imaging systems and predicting their performances an urgent one.

II. BALL SIZE-TIME CURVE

As mentioned above, when imaging with a FIB system, two different "uncertainties" must be taken into account to define the precision with which a feature can be characterized.

(1) Information uncertainty (IU), which depends on the amount of information that is collected from the image (IU$\propto\sqrt{N}$, where N is the number of counts); this term decreases for increasing scan/dwell time (i.e., increasing K).
(2) Sputtering uncertainty (SU), which is due to the fact that atoms from the feature are being sputtered while imaged, changing the size of the feature during the scan; this term increases for increasing scan/dwell time.

The actual resolution of a SIM will be ultimately determined by the competition between these two factors: The first term dominates for high acquisition rates, while the second term is the limiting factor for images taken with a long scan/dwell time.

Further to the theory of Orloff *et al.* outlined in Sec. I A, in this article a practical method of defining the resolution of a SIM is proposed, which does not depend on the implicit assumptions of the cited theory (Poisson-distributed ions and SE, and perfect SE collection efficiency), and takes into ac-

TABLE I. Scan/dwell time and total time for the sets of images used for the analysis.

Set	Scanning time (s)	Dwell time (μs)	No. of scans	Total time (s)
1	6.337	6.487	160	1014
2	11.77	12.048	100	1177
3	22.63	23.165	60	1358
4	45.26	46.330	40	1810
5	90.52	92.661	20	1810
6	162.9	166.753	5	814.5

count not only the uncertainty due to the sputtering but also the one connected with the amount of collected information.

The basic idea is to follow the evolution of a sample under observation with an ion beam. In order to have isotropic features, with only one characteristic size, a Sn-ball sample has been chosen, one of those commonly used for SEM calibration. Such samples are commercially available, in particular, the one used for our experiments is a "universal resolution tin on carbon" from Agar Scientific, with particle diameters ranging from <5 nm to 30 μm. Different sets of images have been recorded, each with a different scan/dwell time ($t_{\mathrm{dwell}}=t_{\mathrm{scan}}/px$), because each scan time corresponds to a different amount of collected signal [see Eq. (3)]. All the images have been taken with a Ga^+ dual-beam (FEI Strata DB 235), with a nominal current of 1 pA and a beam energy of 30 keV. The image size is 1024×954 pixels (the largest

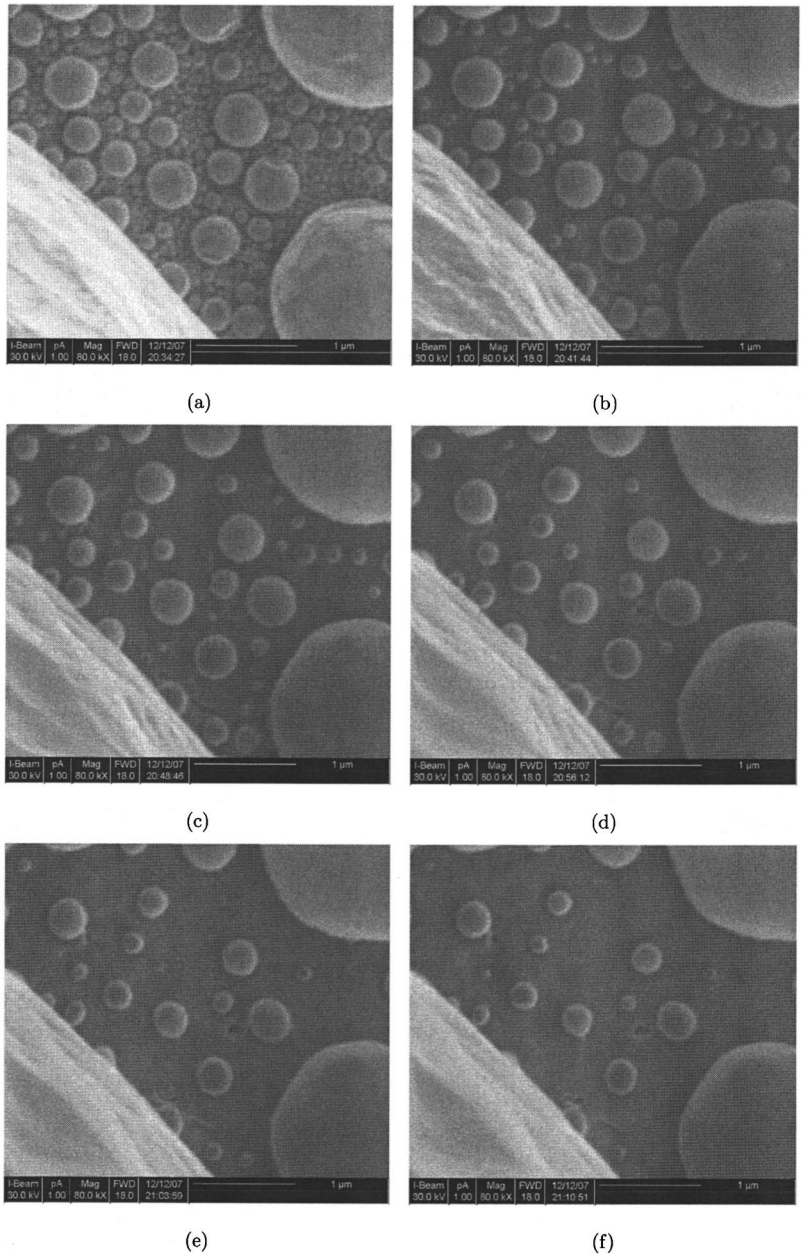

FIG. 2. Time evolution of the Sn-ball sample under ion bombardment shown through six time frames from set 3; the damage is already evident in (b); (a) after ~22 s of imaging; (b) after ~294 s; (c) after ~565 s; (d) after ~837 s; (e) after ~1110 s; (f) after ~1358 s.

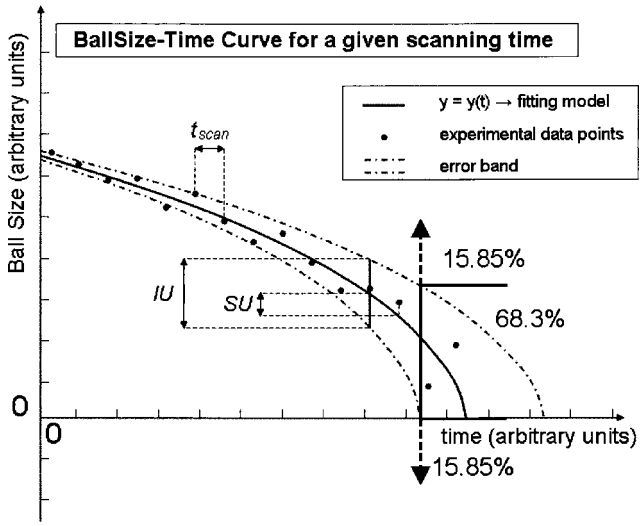

FIG. 3. Ideal appearance of the ball size-time curve; IU is the thickness of the uncertainty band at each point, corresponding to a given confidence level of the measurement (68.3% in this picture); SU is the reduction in size between two successive scans; t_{scan} is the distance between two successive data points.

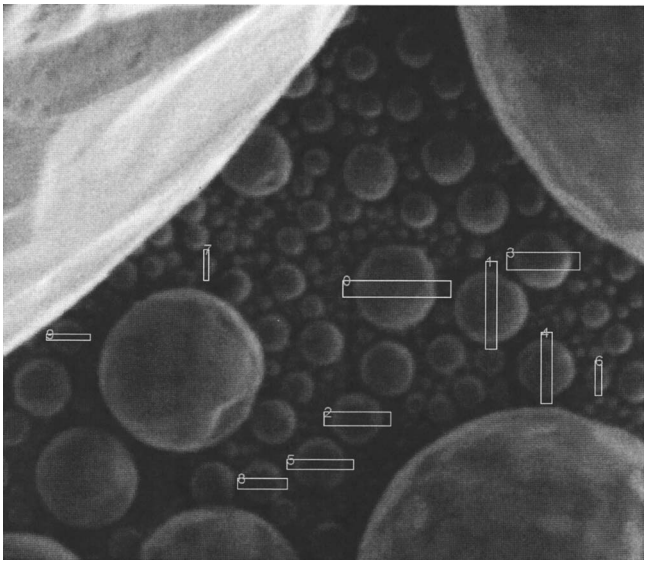

FIG. 4. Features of interest selected on the first frame of the time series; for each ball the diamater is calculated averaging the pixel lines over the width of the selection boxes.

size supported by the machine), with a magnification of 80 k× and a pixel size of 3.7 nm/pixel. The six sets used for the analysis are summarized in Table I. Figure 2 shows the time evolution of the sample under ion bombardment through six frames from set 3, from the first to the last scan; the damage is already evident in Fig. 2(b), and it becomes dramatic in Fig. 2(f).

The image analysis was carried out with the MATLAB toolbox DIPimage. (DIPimage reference website: http://www.diplib.org/). For each set of scans the ball size-time curve for different particles is obtained, which is a plot of the particle' s diameter versus the scan/dwell time. The way such a diagram is expected to look is shown in Fig. 3. The plot also includes the parameter IU, calculated for each point according to the procedure that will be outlined in the next section. In this way, both terms needed to define the resolution appear in the curve.

(1) $\mathrm{SU}=\int_{t^*-\Delta t/2}^{t^*+\Delta t/2} dy/dt(t)dt$, where t^* is a given instant and Δt is the scan time; the derivative is calculated along the curve $y=y(t)$, which fits the experimental data.
(2) $\mathrm{IU}\propto 1/\sqrt{n}$, where n, as it will be shown in Sec. II B 3, is the number of pixel lines on which the diameter of a ball can be assumed constant, and is a function of the current size of the ball.

The main issue here is that

$$\mathrm{SU}=\mathrm{SU}(dy/dt), \quad dy/dt=dy/dt(t) \Rightarrow \mathrm{SU}=\mathrm{SU}(t),$$

$$\mathrm{IU}=\mathrm{IU}(n), \quad n=n(y), \quad y=y(t) \Rightarrow \mathrm{IU}=\mathrm{IU}(t);$$

i.e., none of the two terms are constant along the curve. This problem will be addressed in Sec. IV. In order to plot the curve, the image-analysis procedure must be able to (1) measure the diameter of a chosen particle, for each frame of a set of images; and (2) determine the error that affects the estimation of the diameter, in terms of absolute length.

The second item has a key role in this analysis, and its definition must be set with care.

A. Determination of the particle diameter (*D*)

The measurement of the balls' diameter for each frame of a set of images is performed with a semiautomated algorithm based on second order derivative edge detection.[16] The procedure consists of the following steps.

(1) *Image preprocessing*. Each set must be corrected for the image drift, which is always present in the order of few nanometers for images taken over a time of 15–20 min.
(2) *Feature selection*. In this step the balls of interest are manually selected on the first frame of the set; what is actually selected is a rectangular box comprising the ball's diameter (Fig. 4).
(3) *Averaging*. The intensity levels of each pixel in the box are averaged over the width of the box, in order to obtain a one pixel profile for the length estimation (Sec. II B 3).
(4) *Edge detection*. This is the core of the algorithm; the zeros in the second derivative are found; because with shot noise and shadow effects there can be more zeros than edges, a check on the local maxima and minima is performed in order to select the right points (Fig. 5): Only the two zeros (one per side) with highest distance between the nearest local minima and maxima are identified as edges and selected.
(5) *Refining*. The subpixel positions of the zero crossing are found by interpolation of the second derivative.
(6) *Slope measurement*. For each edge, the slope at half maximum is calculated (See Sec. II B 3).

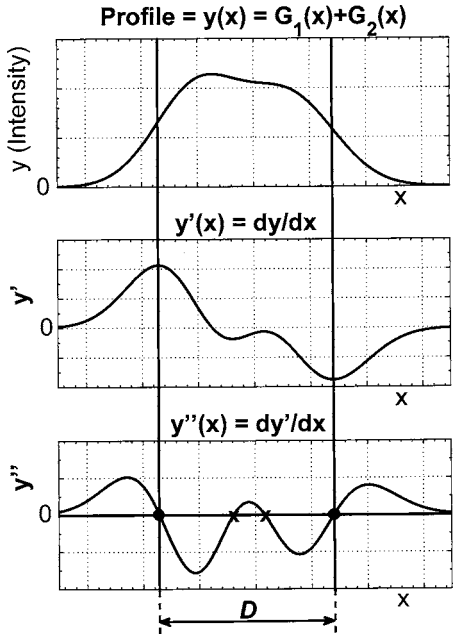

FIG. 5. Edges of the features are found among the zero points of the second derivative of the intensity level; here the simple case of an analytic profile (sum of Gaussians) is shown, in which only the two zeros for which the distance between the nearest local maximum and the nearest local minum is the highest correspond to the edges of the feature.

B. Determination of the information uncertainty (IU)

The term that we have indicated as IU, i.e., the resolution connected with the image acquisition process, depends essentially on three things:

(1) the shot noise, σ, decreasing while increasing the acquisition time;
(2) the slope of the edge of the particle, in the diagram intensity position; and
(3) the *a priori* knowledge available about the feature.

1. Shot noise (σ)

The shot noise σ is intensity dependent and is normally evaluated through different images of the same area. Being this not possible in the case of FIB imaging, an estimation of σ for a given intensity can be obtained as the variance of the gray levels in a flat surface (i.e., an area of the sample void of features); this is shown in Fig. 6 in the monodimensional case. This value of σ must then be corrected for the intensity level of the part of the feature where the size and the slope (see Sec. II B 3) are measured. In order to do this, the variance is evaluated at different (void) positions in the image, each characterized by a different mean gray level: The value of σ corresponding to the intensity level of the feature is then estimated through interpolation.

2. Error on the diameter measurement (ΔD)

The shot noise σ must be converted into an estimation of the uncertainty in the determination of the particle diameter.

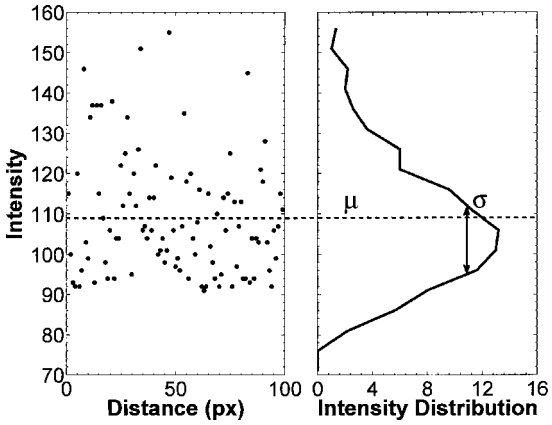

FIG. 6. Shot noise σ is evaluated as the variance of the gray levels in a flat area. Here a monodimensional case: on the left the intensity levels along a straight line, on the right their distribution, with its mean (μ) and standard deviation (σ).

This can be done, once again in a model-independent way, determining the slope at 50% of the step profile. In the general case of an asymmetric profile, the left and right sides must be taken separately into account. With reference to Fig. 7, indicating with D the particle diameter, ΔD can be expressed as:

$$\Delta D = \frac{\Delta D_L + \Delta D_R}{\sqrt{2}} = \frac{\sigma/|\tan\theta_L| + \sigma/|\tan\theta_R|}{\sqrt{2}}. \quad (5)$$

3. Dependence of IU on the feature's size

IU and σ are strictly related, but not exactly coincident. In every measurement process, regarding the result as a stochastic variable, the error is reduced repeating the measure-

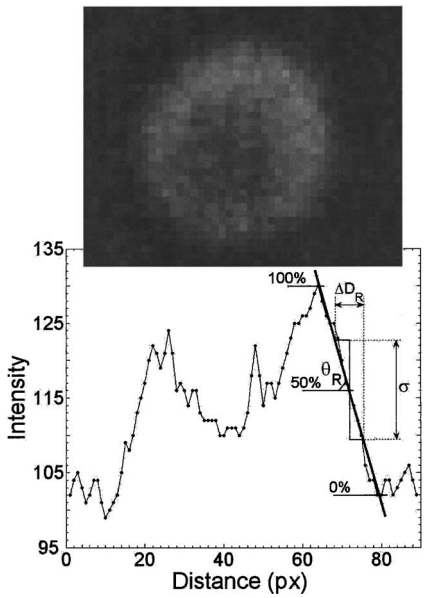

FIG. 7. Evaluation of ΔD as projection of the error band due to the shot noise on the distance axis; for each edge, the slope of the intensity level at half maximum is considered.

ment a certain number of times, and averaging the results. This is not possible in the case of ion imaging, because of the intrinsically destructive nature of the process. Moving around this obstacle is possible exploiting *a priori* knowledge of the system being observed. Suppose we want to estimate the thickness of an $m \times n$ pixel line, a measurement along one pixel column will be affected by an error ΔT, which cannot be reduced, since imaging the same column again for a second measurement would affect the thickness itself, and the value of this second measurement would not represent the same stochastic variable. Nevertheless, if the thickness of the line "is known" to be constant along the whole length (or a part of it), measurements of the thicknesses T_i along different pixel columns would represent different observations of the same random variable, the theoretical thickness T. In this way the error ΔT can be reduced by simply averaging different observations along different pixel columns, being the total number of observations (n) only limited by the length of the line along which the thickness is known to be constant.

The case of a sphere is analogous: The *a priori* knowledge of the feature (assumed as a perfect sphere) suggests that it is possible to average over different diameters. This is theoretically correct, but may not be the best approach in terms of implementation. An approximation is to assume that the diameter is constant for a certain number of adjacent pixel lines (centers on a geometric diameter). This solution has been chosen for different reasons.

(1) It is less affected by the fact that the particle might not be a perfect sphere, or might change its shape during the sputtering because of atomic anisotropy.
(2) It is less affected by aberration effects, in particular, astigmatism.

The number of pixel lines along which the observations of the diameter's length can be averaged is of course a function of the particle's size; it can be assumed, for example, that the diameter is constant for 1/5 of the diameter. If C, in pixel/nm, is the pixel size in the image, the number of observations that can be used to average the measurement, and thus to reduce the error, is

$$n = \lfloor 0.2DC \rfloor + 1. \tag{6}$$

Once the function $n = n(D)$ has been tabulated, it is finally possible to express the "information uncertainty" IU for each point of the ball size-time curve as

$$\frac{\mathrm{IU}}{2}(D) = \frac{\Delta D}{\sqrt{n}} = \frac{\sigma/|\tan\theta_L| + \sigma/|\tan\theta_R|}{\sqrt{2}\lfloor 0.2DC \rfloor + 1}. \tag{7}$$

III. NUMERICAL SIMULATION

While IU, as shown in Eq. (7), depends on the quality of the image through the parameter σ, the sputtering effect on a feature hit by an ion beam, and its shrinking with the time/dose, can be simulated with a numerical approach. The starting point is the sputtering yield Y, defined as the number of target atoms sputtered away for each incident ion. This parameter is strongly dependent on the surface binding energy (SBE) of the target, whose value is sometimes difficult to estimate, and it is usually approximated with the heat of sublimation of the target. The calculation of the sputtering yield has been carried out with TRIM, a free code distributed by Ziegler (SRIM/TRIM reference website: http://www.srim.org/), which implements a Monte Carlo method. The SBE also changes under bombardment due to surface roughness and damage, and, for compounds, also due to changes in the surface stoichiometry, which makes the calculation of Y accurate only to about 30%. Y has been simulated as a function of the incidence angle of the beam on the target surface, α. This dependence is fundamental in the case of a spherical geometry, where the incidence angle of the ion beam is constantly changing along the surface of the feature. For each value of α, between 0° and 89.9° with a step of 1°, the impact of 1000 Ga^+ with an energy of 30 keV has been simulated in order to have a reasonable accurate estimate of Y. The result is shown in Fig. 8.

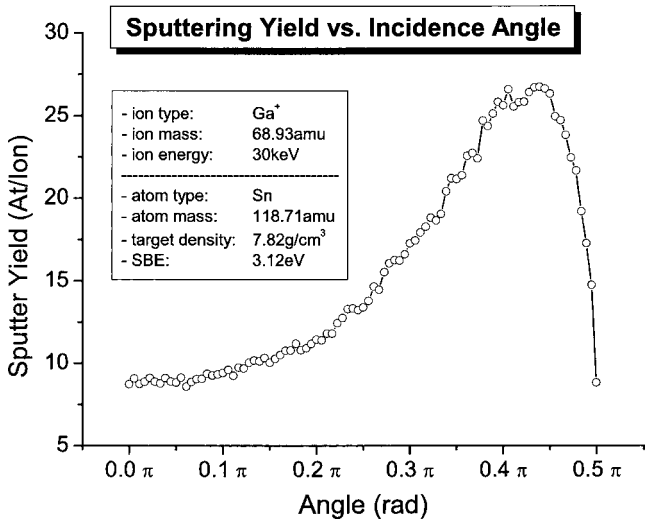

FIG. 8. Sputtering yield vs incidence angle for 30 keV Ga^+ impacting on Sn, as obtained from Monte Carlo simulation using the TRIM code.

Once the sputter yield as a function of α is known, Y can be converted to a sputter rate (SpR), i.e., the pace at which a surface recedes under ion bombardment,

$$\mathrm{SpR}(\alpha) = \frac{4AI}{\pi d^2 e \rho N_0} Y(\alpha), \tag{8}$$

where e is the ions' charge, ρ and A are the target density and the target molecular weight, d is the beam diameter, and I is the beam current. If all the parameters are expressed in S.I. units, SpR will be expressed in m/s.

Indicating with $y_0(x)$ the feature profile before the ion bombardment starts, at each time step Δt the profile of the particle that is being sputtered must be "receded" with the amount SpR Δt; thus, the ball profile at the time $n\Delta t$ is

$$y_{n\Delta t}(x) = y_{(n-1)\Delta t}(x) - \mathrm{SpR}(x)\Delta t. \tag{9}$$

In Eq. (9) SpR has been written as a function of x because α is a function of x. The initial profile $y_0(x)$ can take any

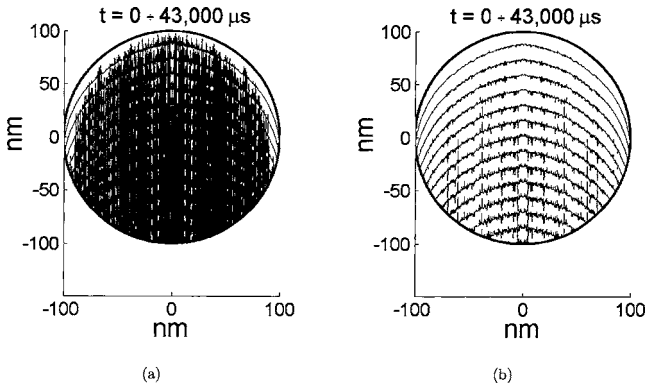

FIG. 9. Evolution, under ion bombardment, of the profile of a Sn ball. In (a) the spikes are due to numerical errors and to the fact that $Y(\alpha(x))$ is not analytical; in (b) the curves have been smothered with a size 3 minimum filter, for an improved visualization.

form; in the case of a spherical feature of radius r, $y_0(x) = \sqrt{r^2 - x^2}$ represents the upper-right quarter of the ball. Recursive application of Eq. (9) gives the profile of the feature as it is changing because of the sputtering effect, as shown in Fig. 9. At each time step, the size of the feature is given by the distance between the intersections of the curve $y_{n\Delta t}(\pm x)$ with the initial profile $-y_0(\pm x)$: The points of the curves $y_{n\Delta t}(\pm x)$ lying below the initial shape must not be considered.

The ball size-time curve calculated in this way is merely numerical; still, it gives an idea of what should be expected in terms of size shrinking of a feature hit by an ion beam. Moreover, the curve appears to be reasonably well fitted by a second order polynomial (Fig. 10).

As mentioned above, this numerical simulation is based on a "continuum" isotropic approach. Therefore, it does not take into account the fact that the target's atoms are differently packed along different crystalline orientations, or the "channeling effect" (i.e., the ion range is higher for specific crystalline directions) is intrinsically nonisotropic. The effect

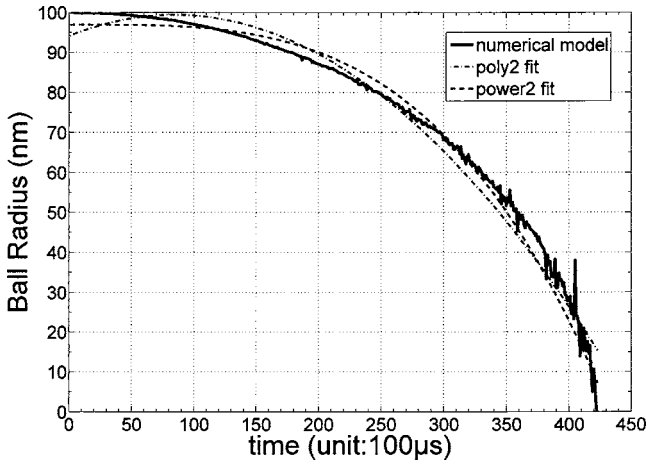

FIG. 10. Ball size-time curve as obtained from Fig. 9(b); fittings with a second order polynomial and with a power function are shown.

of redeposition, which can significantly change the shape assumed by the particles during the sputtering process, is also not considered.

IV. APPLICATION OF THE MODEL AND DISCUSSION

In the previous sections the expressions for both error contributions, the one related to the sputtering and the one related to the amount of collected information, have been shown; IU is given by Eq. (7), while SU is the difference in size of the ball between two scans as follows:

$$\mathrm{SU} = \Delta y = \int_{t^*-\Delta t/2}^{t^*+\Delta t/2} \frac{dy}{dt}(t)dt, \tag{10}$$

where the function $y(t)$ is the fitting model chosen to describe the shrinking of the ball. At this point the model is complete, and can be applied to the sets of images summarized in Table I, in order to define the smallest detectable feature, as follows.

(1) *Image processing and analysis*. To determine the diameter and the slope of the edges, for each time frame; this should be done for each set for particles of similar initial size (Sec. II A).
(2) *Fitting of the experimental data*. A second order polynomial is generally good, while in some cases a more complex one should be chosen (Sec. III).
(3) *Determination of IU*. For each point of the ball size-time curves this is accomplished using Eq. (7).
(4) *Selection of IU and SU (in the limit of the smallest feature) for each set*. As already pointed out in Sec. II, none of these two quantities is constant along the curve. It is still possible, anyway, to define a single value of uncertainty for a given t_{scan} /dose, taking IU and SU at the time $\bar{t}$ for which $y(\bar{t}) = \mathrm{IU}(\bar{t})/2$; this is indeed the smallest diameter that can be measured, because for $y < y(\bar{t})$ the lower limit of the error band would be negative.
(5) *IU versus t_{scan} and SU versus t_{scan}*. A plot of these two curves on the same diagram gives immediate information about the highest accuracy that can be reached when measuring feature sizes with a FIB system.

The procedure was implemented following, for each set of images, the evolution of balls of initial diameter of about 200 nm. Figure 11 shows the ball size-time curves: experimental data points, quadratic fit, and the error band connected to the shot noise. To speed up the calculation, a single value of θ_L and θ_R has been used for each set, which can be justified by the fact that the imaging conditions are exactly the same for all the frames of each set (see Fig. 12). Figure 13 shows the plots, on the same diagram, of SU and IU as a function of the scanning time, evaluated for each curve of Fig. 11 at the time $\bar{t}$ for which the lower limit of the error band becomes zero. The value of t_{scan} corresponding to the intersection of $\mathrm{IU}(t_{\mathrm{scan}})$ and $\mathrm{SU}(t_{\mathrm{scan}})$, $\bar{t}_{\mathrm{scan}}$ is the scanning time for which both the information uncertainty and the sputtering uncertainty are minimized and represents, therefore, the best operating condition. It must be pointed out that IU

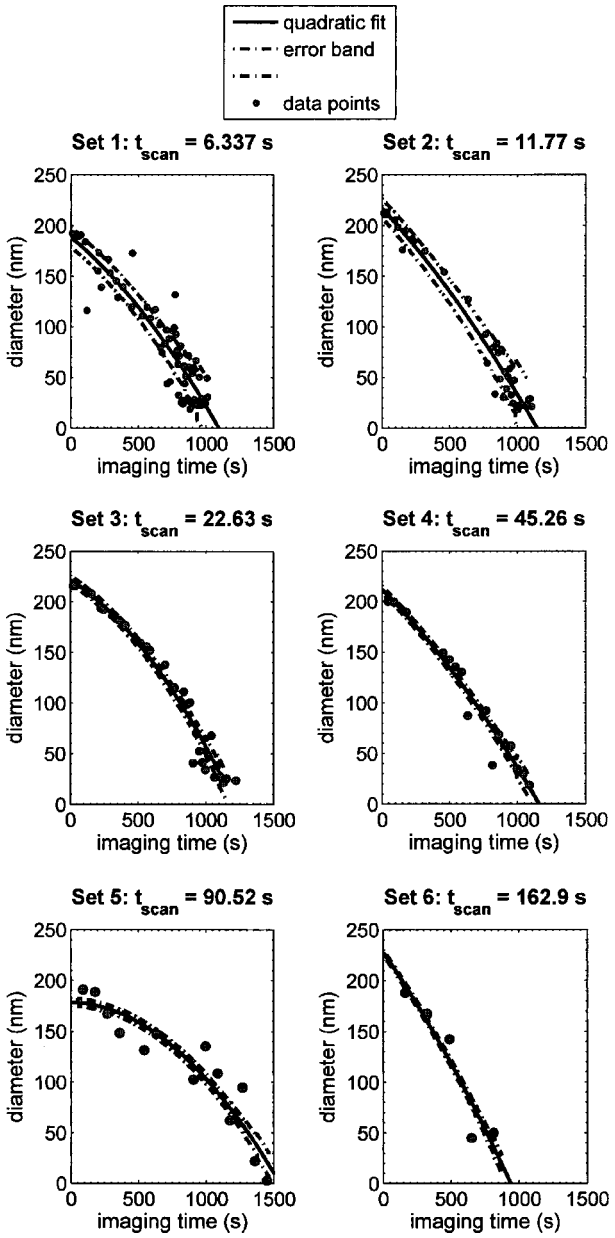

FIG. 11. Ball size-time curves for each of the six sets of images, for balls of approximately equal initial diameter (~200 nm); each diagram shows experimental data points, quadratic fit, and error band connected to the noise.

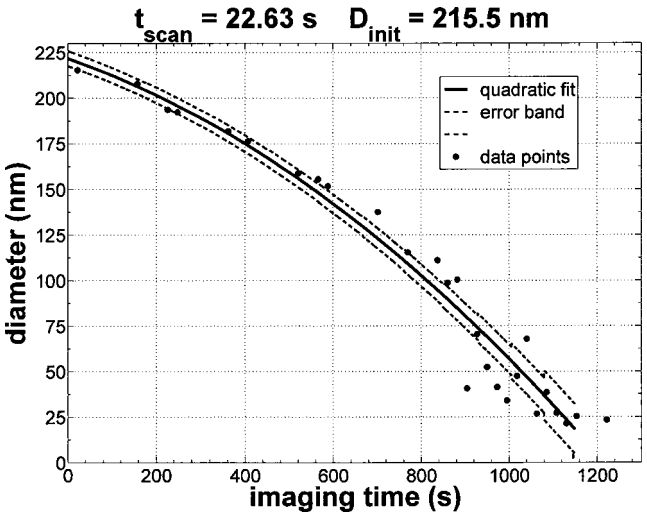

FIG. 12. Third curve of Fig. 11 for a better visualization; the initial diameter of the ball is ~215.5 nm, and the feature totally disappears after ~1200 s of scanning with a current of 1 pA.

relates to the variance σ of the gray level distribution in a flat area (Sec. II B 1), i.e., it relates to a given accuracy of the measurement. Assuming Gaussian-distributed gray levels (a good approximation for a high number of counts/pixels), the choice of 1σ returns a confidence level of 68.3%. This means that if y^* is the best estimation for the particle's diameter at the time t^*, the probability for the particle's diameter to be in the range $[y^*-\mathrm{IU}(t^*)/2,\ y^*+\mathrm{IU}(t^*)/2]$ is 68.3%. Referring to Fig. 3, the statement that $y(\bar{y})$ is the smallest measurable diameter implies the assumption that such minimum diameter is the one for which the probability to still observe "something" is 84.15%. If 84.15% is found to be too low, or too high, the analysis may be implemented for a different confidence level.

From our experiments we found a best scanning time close to 100 s, corresponding to IU=SU=23 nm. This means that using a FIB with those imaging conditions (focus, astigmatism, etc.) will give a precision in terms of measurement of features not higher than ± 11.5 nm, a value that is achieved only using 100 s to take a single picture; scanning for less than 100 s will give higher uncertainty because of the insufficient collected information, while for scanning times >100 s the sputtering effect will be the limiting factor: The collected information is not exploited because the reduction of feature's size during the scan is higher than IU.

It is interesting to observe that, from Eq. (3), a scanning time of 100 s, assuming $\delta=2$ and $\Omega=0.5$, corresponds to a SNR $K\sim 26$, which in turn, using Eq. (1) or Eq. (4), or simply looking at the diagram in Fig. 1, gives a minimum detectable feature size of ~12 nm (for a sputtering sensitiv-

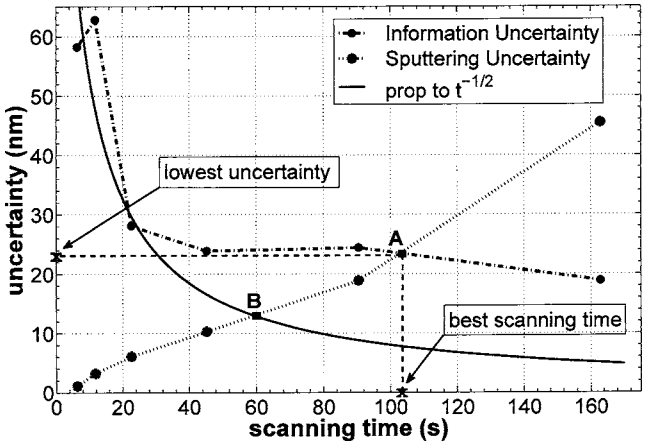

FIG. 13. Plot of SU (t_{scan}) and IU (t_{scan}) on the same diagram gives an immediate evaluation of the best scanning time and the corresponding best accuracy that can be achieved in a measurement (for given imaging conditions) in a FIB imaging system. The solid line represents an "ideal" IU curve, for which the uncertainty is pure shot noise.

ity of 2 $\mu m^2/nC$). This is surprisingly close to the minimum uncertainty obtained with our analysis, considering that the two values have been obtained with two completely different methods, and the fact that the theory of Orloff does not take into account the redeposition (which is implicitely included in our experimental approach) or the dependence of the sputtering sensitivity on the incidence angle of the beam.

Some considerations about $IU(t_{scan})$ and $SU(t_{scan})$ are needed. As it appears from Eq. (10), IU depends on the shape of the feature being observed, ultimately because the sputtering is a strong function of the incidence angle. This means that the optimum scanning time $\bar{t}_{scan}$ will be different for different samples. Even when all features have the same initial shape, like in the case of the Sn balls, care must be taken in defining the optimum operating conditions; balls of different initial diameters will have different ball size-time curves, and thus different SU, because the shape changes from a sphere to a disk (Fig. 9): A feature of initial diameter, for example, of 100 nm, once reduced by the sputtering to a diameter of 50 nm, will be different from a feature whose initial diameter is 50 nm. About IU, it must not be forgotten that while the term σ is in principle only related to the scanning time, the slope of the feature's edge, θ, can be different for different imaging conditions, such as focus and astigmatism. These parameters can also affect $\bar{t}_{scan}$.

Figure 13 shows how the sputtering and the collection of information compete to determine the smallest observable feature. Assuming shot noise limited information collection, IU should follow the $1/\sqrt{t_{scan}}$ curve shown as a solid line. It is clear that due to some other factors there is a deviation, whose effect is to reduce the smallest observable feature dependence with the sputtering. We espect that under more favorable conditions the IU curve will follow for longer the shot noise limited curve; thus, the intersection point moves from point *A* to point *B*, where the slope of the IU curve is greater, and so the dependence on the sputtering.

V. CONCLUSIONS

In this article a procedure for finding the best scanning time and the corresponding minimum measurement error when imaging with a FIB system is proposed. The approach is experimental, and complements the theory of sputtering developed by Orloff *et al.* The procedure is based on following the shrinking of spherical features while imaging with the ion beam, and has been tested on six different sets of images, each one with a different scanning time. As a result we plotted the measurement error connected with the collection of signal (SE) and the error connected to the change in the feature's size due to the sputtering, both as a function of the scanning time. For the imaging condition under which our pictures were taken, we found a best scanning time of ~100 s, and a minimum error of ~23 nm, a value that is not far from the minimum detectable size obtained by Orloff for the same SNR. The minimum error and the best scanning time are both dependent on the imaging conditions: Assuming that parameters such as focus and astigmatism were not optimized during our experiments, it is reasonable to assume that the curve $IU=IU(t_{scan})$ can be moved toward smaller values, bringing the minimum error even closer to the theoretical sputter-limited resolution.

The analysis of the performances of a FIB system is interesting especially because of the fact that different new ion sources are now appearing or are being studied, for which the expectation, for the scientific community and for the industry, is very high.

ACKNOWLEDGMENTS

This work is part of the research programme "Microscopy and Modification of NanoStructures With Focused Electron and Ion Beams" (MMN) of the "Stichting voor Fundamenteel Onderzoek der Materie," which is financially supported by the "Nederlandse Organisatie voor Wetenschappelijk Onderzoek." The MMN programme is cofinanced by FEI Company.

[1] R. L. Seliger, J. W. Ward, V. Wang, and R. L. Kubena, Appl. Phys. Lett. **34**, 310 (1979).
[2] J. Orloff, Rev. Sci. Instrum. **64**, 1105 (1993).
[3] J. Orloff, M. Utlaut, and L. W. Swanson, *High Resolution Focused Ion Beams* (Kluwer, Dordrecht, 2003).
[4] K. Ohya and T. Ishitani, J. Electron Microsc. **52**, 291 (2003).
[5] T. Ishitani and K. Ohya, Scanning **25**, 201 (2003).
[6] K. Ohya and T. Ishitani, J. Electron Microsc. **53**, 229 (2004).
[7] T. Ishitani, Y. Madokoro, M. Nakagawa, and K. Ohya, J. Electron Microsc. **51**, 207 (2002).
[8] J. Orloff, Proc. SPIE **2522**, 412 (1995).
[9] J. Orloff, L. W. Swanson, and M. Utlaut, J. Vac. Sci. Technol. B **14**, 3759 (1996).
[10] Lord Rayleigh, Philos. Mag. **8**, 261 (1879).
[11] J. E. Barth and P. Kruit, Optik (Stuttgart) **101**, 101 (1996).
[12] X. R. Jiang, J. E. Barth, and P. Kruit, J. Vac. Sci. Technol. B **14**, 747 (1996).
[13] J. E. Barth and M. D. Nykerk, Nucl. Instrum. Methods Phys. Res. A **427**, 86 (1999).
[14] V. N. Tondare, Ph.D. thesis, Delft University of Technology, The Netherlands.
[15] B. Ward, J. A. Notte, and N. P. Economou, J. Vac. Sci. Technol. B **24**, 2871 (2006).
[16] P. W. Verbeek and L. J. van Vliet, IEEE Trans. Pattern Anal. Mach. Intell. **16**, 726 (1994).